Available online at www.sciencedirect.com
SCIENCE DIRECT®
Materials Chemistry and Physics 81 (2003) 134–142
MATERIALS CHEMISTRY AND PHYSICS
www.elsevier.com/locate/matchemphys

Electrical conductivity and microstructures of $La_{0.65}Sr_{0.3}MnO_3$–8 mol% yttria-stabilized zirconia

Chih-Chung T. Yang [a], Wen-Cheng J. Wei [a,*], Andreas Roosen [b]

[a] *Institute of Materials Science and Engineering, National Taiwan University, 1 Roosevelt Road, Section 4, Taipei 10617, Taiwan, ROC*
[b] *Department of Materials Science, Glass and Ceramics, University of Erlangen-Nuremberg, D-91054 Erlangen, Germany*

Received 3 December 2002; received in revised form 10 March 2003; accepted 14 March 2003

Abstract

The electrical conductivity and microstructure of $La_{0.65}Sr_{0.3}MnO_3$ (LSM)–8 mol% yttria-stabilized zirconia (YSZ) cathode composite were investigated from room temperature to 1000 °C in air conditions. The results show that dense YSZ, containing 7.52 ± 0.15 mol% Y_2O_3 composes of equiaxed grains. Little glassy phase, consisted of SiO_2 with minor Al_2O_3, is found in YSZ. Two conducting species are responsible for the conduction of YSZ in low and high temperature ranges. One is $Y'_{Zr}V_O^{\bullet\bullet}$ with higher activation energy of 103 kJ mol^{-1} below 550 °C and the other is $V_O^{\bullet\bullet}$ with lower activation energy of 93 kJ mol^{-1} above 550 °C. The transition temperature decreases from 550 to 400 °C for the composites with 10 or 20 vol.% LSM–YSZ. The LSM phase and YSZ dominates the electrical conductivity of composites below and above 400 °C, respectively. As the percolation limit is reached (≥20 vol.% LSM), the electrical conductivity of the composites is determined by LSM phase. The effect of secondary phases on electrical conductivity is insignificant even sintering at 1400 °C for 24 h.

Keywords: Conductivity; YSZ; LSM

1. Introduction

Cathode polarization is the main factor affecting the performance of solid oxide fuel cells (SOFCs) [1,2]. In order to reduce the cathode over-potential, the structure at the interface between $La_{1-x}Sr_xMnO_3$ (LSM) and yttria-stabilized zirconia (YSZ) is modified to provide the higher degree of triple phase boundaries (TPBs). Cathode materials with mixed ionic and electronic conduction (MIEC) offer better electrochemical performances for SOFC because the reduction of oxygen not only occurs at the TPBs but also over the entire surface of the electrode [3]. It was reported [1–5] that LSM–YSZ cathode composite and NiO–YSZ anode composite have been used as cathode and anode materials for SOFCs. However, the formation of secondary phases when YSZ contacts with LSM at higher temperatures had been reported [6–12]. $La_2Zr_2O_7$ (LZ) and $SrZrO_3$ (SZ) are the two reaction products either for a low Sr content ($x < 0.3$) or a higher Sr addition ($x > 0.3$) found at the interface of YSZ–LSM. The electrical conductivity of both zirconates is far lower than that of YSZ, leading to the degradation of SOFC [13,14].

Our previous work [12] has confirmed that the diffusion of Mn controls the formation of the secondary phases. The objectives of the present research are to correlate the relationship between microstructure and electrical conductivity of LSM–YSZ cathode composite and to show the effects of secondary phases on electrical conductivity in dependence of processing conditions.

2. Experimental procedure

2.1. Sample preparation

8 mol% YSZ (TZ-8Y, Tosoh Inc., Japan) and A-site deficient $La_{0.65}Sr_{0.3}MnO_3$ (LSM, Juelich Research Center, Germany) powders were used. The powders of YSZ, LSM and mixtures of LSZ–YSZ (10, 20, 30, 40, and 50 vol.%) were dispersed in *iso*-propanol with 2 mass% dispersant[1] (Hypermer LP-1, ICI Surfactant Inc., USA) and milled for 4 h. After well homogenization by a turbo-mixer, the slurry was

* Corresponding author.
E-mail address: wjwei@ccms.ntu.edu.tw (W.-C.J. Wei).

[1] Based on powder mass.

0254-0584/03/$ – see front matter © 2003 Elsevier Science B.V. All rights reserved.
doi:10.1016/S0254-0584(03)00158-5

dried by a vacuum evaporator at a pressure of 137 mbar for 3 h and then placed in an oven for drying for 24 h. The powders were ground in a mortar with a pestle, and sieved to pass −100 mesh. Two geometries of specimens were prepared for the electrical conductivity measurement. One was a test bar in the dimension of 50 mm × 6 mm × 5 mm and the other was a disk with 25 mm in diameter and 2 mm in thickness. The powder was die-pressed at 42 MPa uniaxially and then sintered at 1400 °C for 1–24 h. The sintered density of specimens should achieve 95% T.D. at least in order to prevent the contamination of painted Pt paste into the specimens through the open pores.

2.2. Electrical conductivity measurement

The electrical conductivity of YSZ, LSM and mixture of LSM–YSZ specimens was measured either by two-point (or four-point) probe DC method or ac impedance spectroscopy. The surfaces of these sintered specimens were polished with a SiC paper (200 mesh) to improve the adhesion of Pt paste, which was painted on the surface of these specimens homogeneously and used as electrodes to reduce the contact resistance of sintered specimens. The electrode area was 0.785 cm^2 for disk specimens and 0.25 cm^2 for test bar specimens, respectively. Two- and four-point probe DC measurements were carried out with an electrometer/high resistance meter (Keithley 6517A, Keithley Inc., USA) and an ampermeter 199 system DMM/scanner (Keithley 199, Keithley Inc.) for high resistive materials and high conductive materials, respectively.

The applied voltage was from ±1.0 to ±10.0 V for low temperature region (≤500 °C) and ±0.10 to ±1.00 V for high temperature region (500–1000 °C) in compliance with the equipment limitation. The ac impedance spectrometer (HP 4284A, HP Inc., USA) with a two-probe method was used to obtain the Cole–Cole plots. The frequency ranged from 20 Hz to 1 MHz with an applied voltage of 1.0 V to the device under the test. All conductivity measurements were performed in air conditions.

2.3. Microstructural characterization

The density of the specimens was measured by Archimedes' method. The polished YSZ specimen was thermally etched at 1280 °C for 20 min to reveal the grain boundary of YSZ grains. The Y_2O_3 content of YSZ was measured while keeping the analysis parameters constant.[2] The experimental details for the analysis of the Y_2O_3 content in 3Y-YZP were reported previously [15]. The phase was identified by X-ray diffractometer (Philips PW1830, Philips Instrument Inc., Netherlands) using Cu Kα radiation. The applied voltage and current were 30 kV and 20 mA, respectively. The scan speed was 2° min^{-1}. The microstructure was examined by scanning electron microscope (LX-30, Philips Instrument Inc., Netherlands) equipped with energy-dispersive spectroscope (DX4, EDAX Corp., USA). Thin foils of 3 mm diameter of specimens were prepared and examined by transmission electron microscope (TEM 100 CXII, JEOL Co., Japan) and analytical electron microscope (HF-2000 FE-TEM, Hitachi Corp., Japan and Tecnai 300 FE-TEM, Philips Instrument Inc., Netherlands) equipped with EDS (DX4, EDAX Corp., USA).

[2] The parameters included accelerating voltage (30 kV), magnification (2000×), working distance (10 mm), tilting angle (15°) and take-off angle (45.3°).

3. Results and discussion

3.1. Characterization of YSZ and LSM

Fig. 1 shows the SEM image of the YSZ specimen, which was sintered at 1400 °C for 1 h. Dense YSZ specimens with equiaxial grains are obtained. Around 2% intra- or inter-granular pores are found. Moreover, the average grain size of YSZ sintered bodies is 5.5 μm. Furthermore, Fig. 2 shows the statistics of Y_2O_3 content in YSZ. It is reported that the amount of cubic phase may affect the electrical conductivity of 8 mol% yttria-stabilized zirconia [16]. Besides, the ionic conductivity of cubic phase YSZ mainly depends on the amount of Y_2O_3 content [16,17]. Therefore, it is important to characterize the Y_2O_3 content in the cubic phase. The result shows that the average Y_2O_3 content is 7.52 ± 0.15 mol%. The variation of Y_2O_3 content could be related to the grain size distribution of YSZ, as shown in Fig. 3. The average grain size is 5.5 μm and grain size distribution is from 1.0 to 13.0 μm. Generally, the grain size of YSZ increases with increasing the Y_2O_3 content while the sintering temperature and holding time is fixed. In the present research, the smaller grains with a lower Y_2O_3 content is found while the larger ones with a relatively higher Y_2O_3 content is observed. The result is consistent with our previous publication [15].

Fig. 4 shows the morphology and composition of a glassy pocket, indicated by "G", which was found in YSZ. The EDS result (Fig. 4b) shows that the composition of the glassy phase is primarily composed of SiO_2 with minor Al_2O_3. ZrO_2 and Y_2O_3 peaks are also observed which may result from the artificial effect due to electron beam scattering. The three dihedral angles of the glassy pocket are less than 120°, implying the glassy film may wet along the grain boundary of YSZ grains. The articles [18–20] have proven that the presence of an insulating glassy film (e.g. SiO_2 glass) on the grain boundaries of YSZ grains results in a decrease in grain boundary conductivity. Basically, the grain boundary conductivity is controlled by the type of oxide, grain size, porosity and impurities, etc. [16]. Since the grain boundary conductivity is dominated by the transport property of O^{2-} in a lower temperature range (<600 °C), the synthesis and

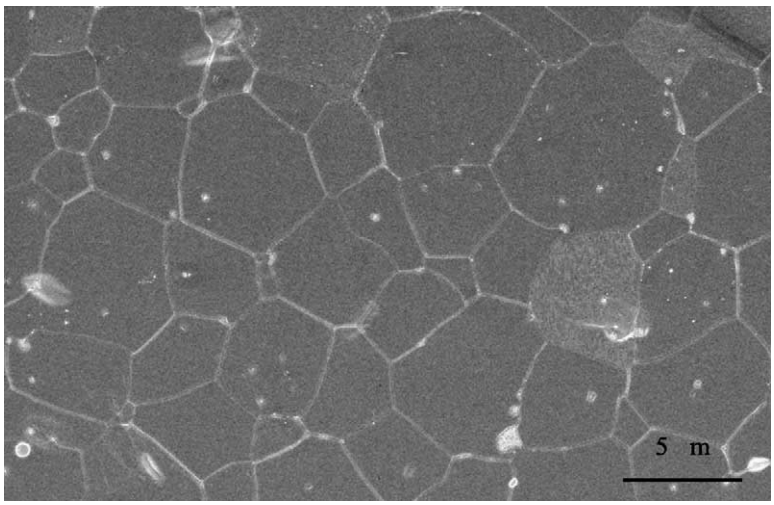

Fig. 1. SEM image of 8 mol% YSZ, sintered at 1400 °C for 1 h.

processing improvements to reduce the amount of glassy phase in YSZ specimens may lead to an increase of electrical conductivity at lower temperatures.

Fig. 5 shows the centered dark field TEM micrograph and diffraction pattern of LSM, which was sintered at 1400 °C for 1 h. The average size of LSM is about 4 μm. The TEM image also shows that some point defect clusters are formed. The diffraction pattern of LSM not only shows the typical diffraction spot of LSM but also the ring pattern, which could be due to the contribution of defect clusters.

3.2. Electrical conductivity of YSZ

3.2.1. DC measurement

It is well known that the addition of Y_2O_3 to ZrO_2 not only stabilizes the cubic phase YSZ, but also enhances the

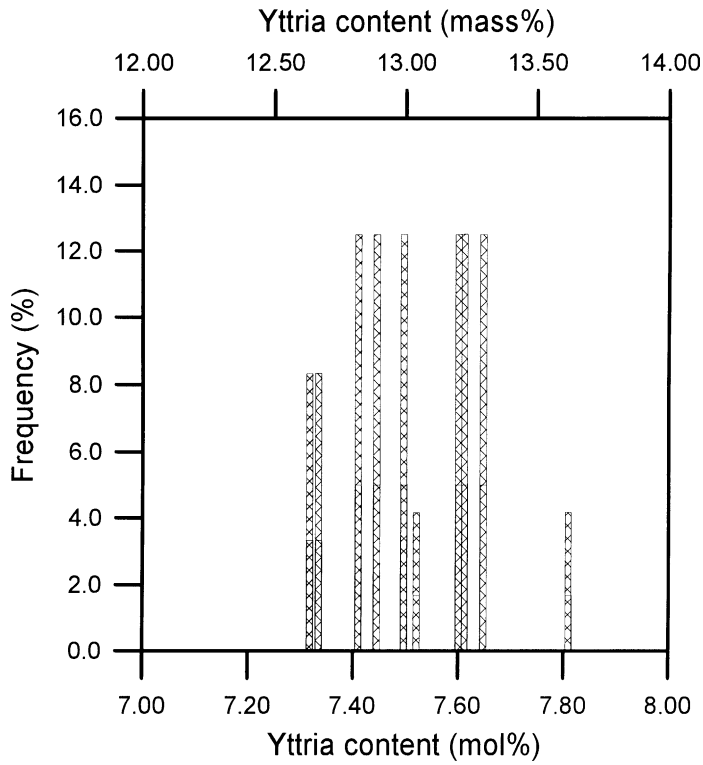

Fig. 2. The distribution of Y_2O_3 content of YSZ specimen, sintered at 1400 °C for 1 h.

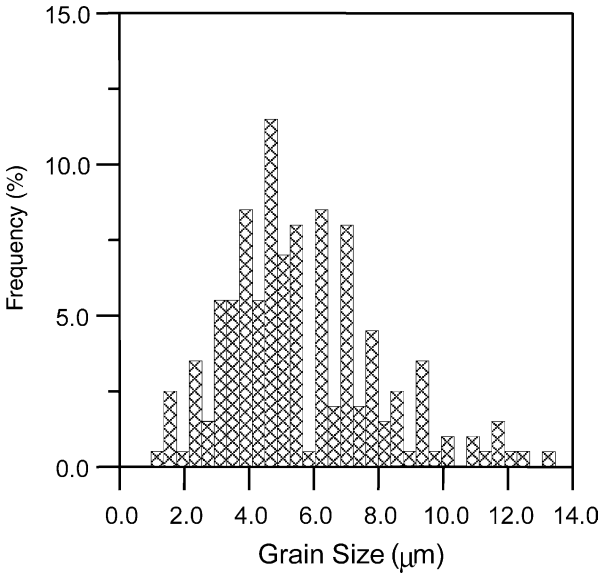

Fig. 3. The grain size distribution of YSZ specimen, sintered at 1400 °C for 1 h.

concentration of oxygen vacancy. The replacement of Zr by Y is compensated by the charges of $V_O^{\bullet\bullet}$. The defect reaction is expressed as

$$Y_2O_3 \overset{ZrO_2}{\rightarrow} 2Y'_{Zr} + 3O_O^x + V_O^{\bullet\bullet} \quad (1)$$

The addition of 7.52 mol% Y_2O_3 to ZrO_2 yields 3.76 mol% oxygen vacancies. Literature [21] reported that the addition of 8–10 mol% Y_2O_3 to ZrO_2 results in the optimum electrical conductivity. At higher temperatures, those oxygen vacancies become mobile. The relationship between

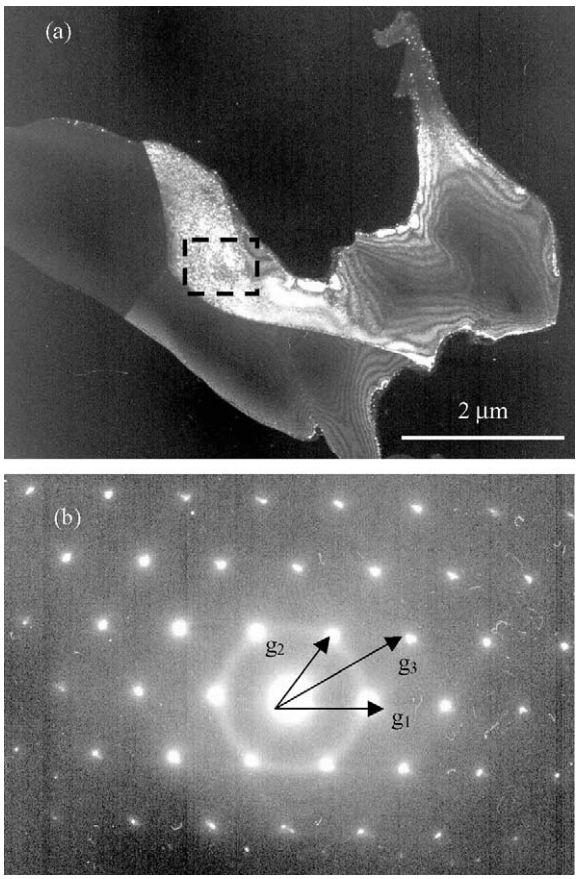

Fig. 5. TEM image and diffraction pattern of bulky LSM specimen, sintered at 1400 °C for 1 h. Note that $g_1 = [1\,0\,1]$, $g_2 = [1\,1\,0]$, $g_3 = [2\,1\,1]$, and zone axis is $[1\,\bar{1}\,\bar{1}]$.

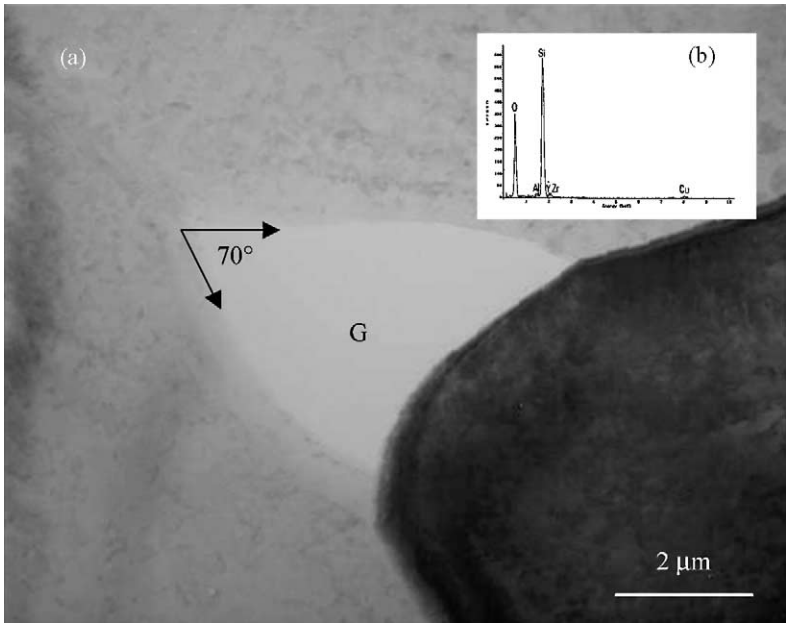

Fig. 4. (a) TEM morphology and (b) EDS spectrum of a glassy pocket, located at triple junction of ZrO_2 grains.

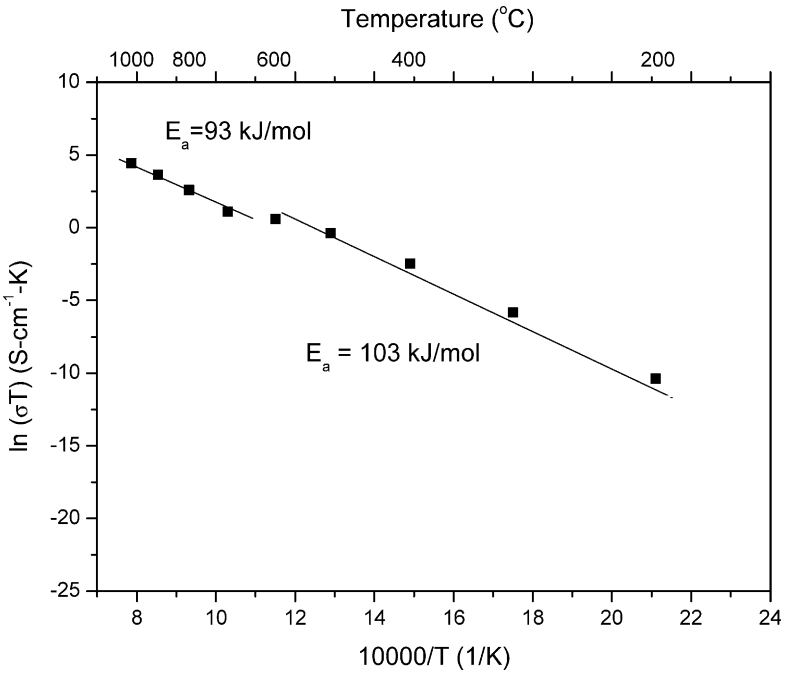

Fig. 6. The electrical conductivity of YSZ as a function of reciprocal absolute temperature.

electrical conductivity and temperature can be described by a thermally activated Arrhenius equation and expressed as

$$\sigma = \left(\frac{A}{T}\right) \exp\left(-\frac{E_a}{RT}\right) \quad (2)$$

where A is the pre-exponential factor, R is the gas constant, and E_a is the activation energy for conduction.

Fig. 6 shows the electrical conductivity as a function of reciprocal absolute temperature. The testing temperature ranges from 200 to 1000 °C. The result shows that a change in slope is observed at around 550 °C, implying the change in conduction mechanism. The activation energy for the conduction above 550 °C is 93 and 103 kJ mol^{-1} below 550 °C, respectively. Filal et al. reported similar activation energy of 111 kJ mol^{-1} and that of 89 kJ mol^{-1} below and above the transition temperature for 9.5 mol% Y_2O_3-doped ZrO_2 [21]. A change in conduction mechanism has been observed. Petot et al. [17] reported that the higher activation energy at low temperatures for conduction is due to the association of the point defects ($Y'_{Zr}V_O^{\bullet\bullet}$). The reason for the lower activation energy for conduction at temperatures higher than 550 °C is due to the migration of $V_O^{\bullet\bullet}$. The electrical conductivity of YSZ is 6.67×10^{-2} S cm^{-1} at 1000 °C, which is close to those reported in literatures [17,19,21].

3.2.2. The ac impedance

The impedance spectra of YSZ, measured at 200, 500, and 1000 °C in air conditions, are shown in Fig. 7. The result shows two semi-circles in the Cole–Cole plot in the lower temperature region (<550 °C), as shown in the inset (Fig. 7a). The semi-circle at high frequency is associated with grain boundary impedance of YSZ while the semi-circle at low frequency is associated with the Pt electrode impedance [22]. The impedance decreases with increasing the temperature. As the temperature increases from 200 to 500 °C, disappearance of grain boundary arc is observed and another semi-circle contributed from grain interior starts to dominate the electrical conductivity, as shown in the inset (Fig. 7b). Only one semi-circle (Fig. 7c) is found when measuring at 1000 °C, illustrating the grain interior makes the contribution to electrical conductivity. It is noted that the ionic conduction of YSZ below and above 550 °C shows different conduction mechanisms.

3.3. Electrical conductivity of LSM

Fig. 8 shows the product of conductivity and absolute temperature as a function of reciprocal absolute temperature. The LSM was sintered at 1400 °C for 1 h. The result shows the activation energy for conduction is 9.6 kJ mol^{-1} in the testing temperature range. Only one conduction mechanism may be dominant in LSM specimens from 200 to 1000 °C. The electrical conductivity of LSM at 200 °C is 2.08 S cm^{-1} and increases to 3.5 S cm^{-1} at 1000 °C.

The addition of Sr^{2+} to La^{3+} in A-site causes the changes in oxidation states of Mn ions. The electrical conductivity of LSM is controlled by the Sr^{2+} substitution for La^{3+} [8]. It is well known that the Mn ions can be divalent, trivalent or tetravalent [23]. The Mn ions tend to exist in the form of Mn^{3+} in the atmospheric conditions. The Sr^{2+} substitution for La^{3+} can be consequently compensated by either

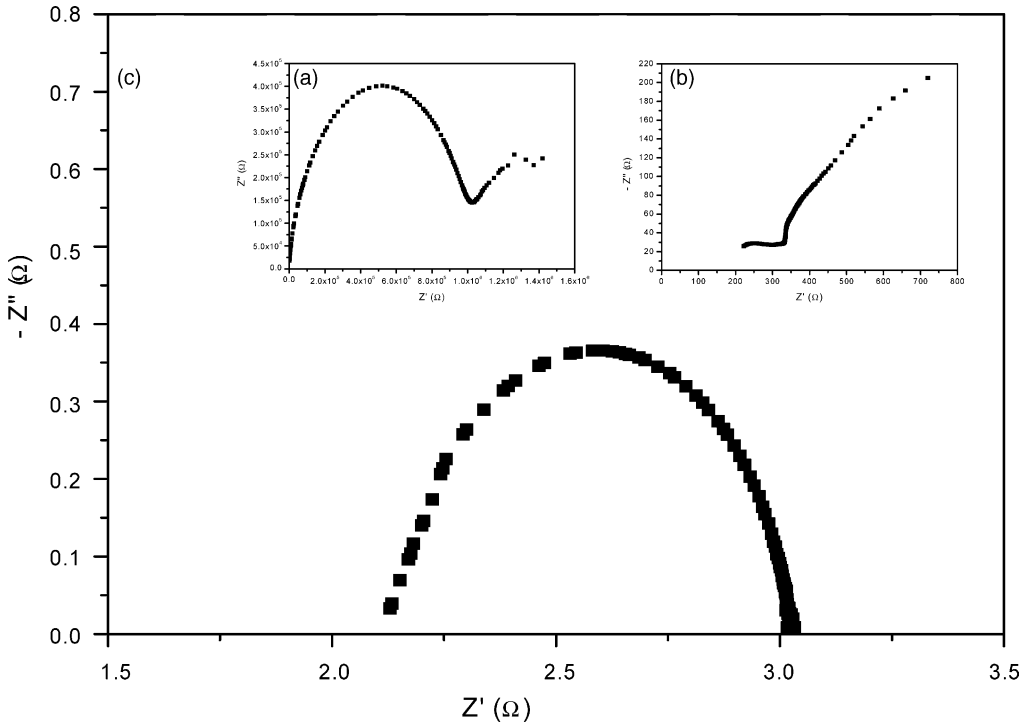

Fig. 7. The ac impedance spectra of YSZ, measured from (a) 200 °C; (b) 500 °C; and (c) 1000 °C in air conditions.

electron hole ($h^{\bullet}$) or oxygen vacancy ($V_O^{\bullet\bullet}$). The possible defect equations are as follows:

$$2SrO + Mn_2O_3 + \tfrac{1}{2}O_2\,(g) \xrightarrow{LaMnO_3} 2Sr'_{La} + 2Mn^x_{Mn} + 6O^x_O + 2h^{\bullet} \quad (3)$$

or

$$2SrO + Mn_2O_3 \xrightarrow{LaMnO_3} 2Sr'_{La} + 2Mn^x_{Mn} + 5O^x_O + V_O^{\bullet\bullet} \quad (4)$$

The oxidation of Mn^{3+} into Mn^{4+} takes place in order to maintain local electrical charge equilibrium. The Sr

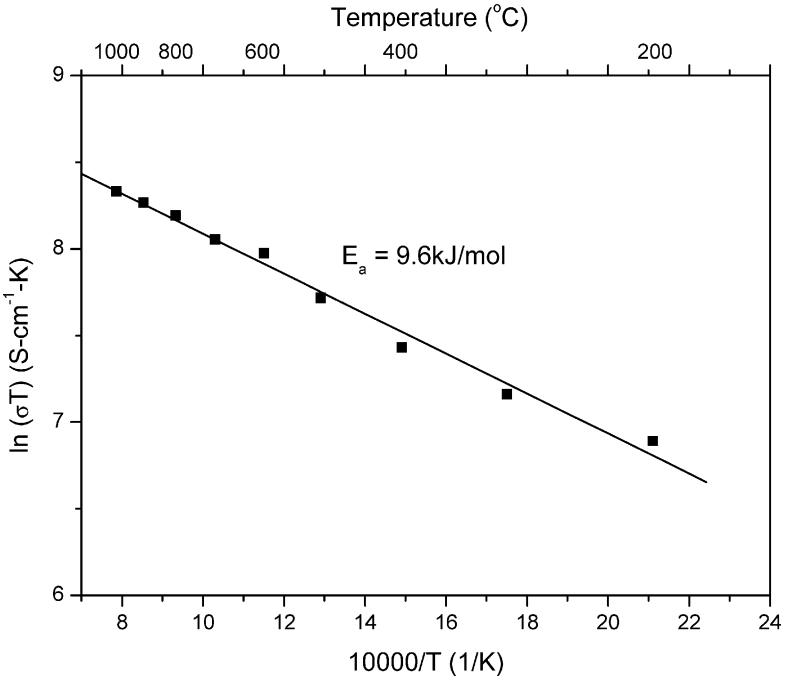

Fig. 8. The electrical conductivity of LSM as a function of reciprocal absolute temperature.

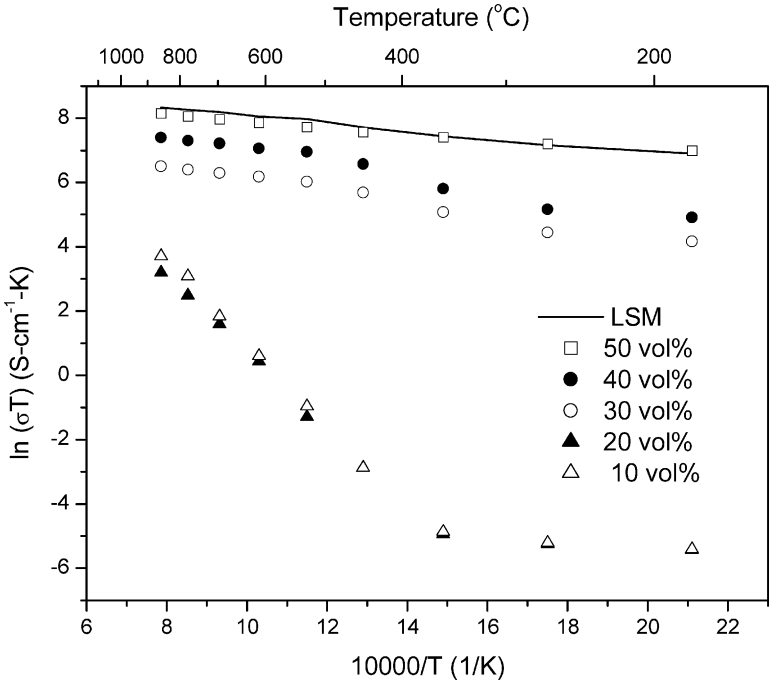

Fig. 9. The electrical conductivity as a function of temperatures for various LSM–YSZ cathode composites, sintered at 1400 °C for 24 h. The solid line is the data of pure LSM as shown in Fig. 8.

substitution for La enhances the electrical conductivity of LSM by increasing the concentration of Mn^{4+}, owing to the combination of Mn^{3+} and $h^{\bullet}$. The Mn^{4+} ion can be regarded as a Mn^{3+} ion, which is associated with a positively charged hole. The $h^{\bullet}$ can separate from the associated defect ($Mn^{3+}\cdot h^{\bullet}$) easily. Moreover, oxygen vacancy could be another charge compensation for the replacement of La by Sr in LSM system. The formation of oxygen vacancy always carries an electron in terms of electroneutrality and the negatively charged electron makes the Mn^{4+} reduce to Mn^{3+}. The reduction of Mn^{4+} to Mn^{3+}, which is related to oxygen desorption, favors the formation of oxygen vacancy. The combined oxidation of Mn^{3+} to Mn^{4+} and formation of oxygen vacancy can be expressed as

$$2Mn^{4+} + O_O^x \leftrightarrow \tfrac{1}{2}O_2\,(g) + V_O^{\bullet\bullet} + 2Mn^{3+} \quad (5)$$

Wu et al. [24] reported that the oxidation of Mn^{3+} to Mn^{4+} and formation of oxygen vacancy both take place in $La_{1-x}Ca_xMnO_3$ (LCM) system for NH_3 oxidation. Therefore, it is believed that both the charged hole and oxygen vacancy may make the contribution to the electrical conductivity of LSM in the present research.

3.4. Properties of LSM–YSZ cathode composite

In order to investigate the conductive behavior of LSM–YSZ composites, the specimens with different ratios from 10 to 50 vol.% LSM were sintered at 1400 °C for 24 h. Fig. 9 shows the conductivity of a series of LSM–YSZ composites as a function of reciprocal absolute temperature. The results indicate two conduction mechanisms are operated for 10 and 20 vol.% LSM–YSZ cathode composites. For LSM–YSZ composites containing lower LSM phase such as 10 and 20 vol.% LSM, the oxygen vacancy of YSZ controls the transport at temperatures higher than 400 °C while the hole of LSM dominates the conduction at temperatures below 400 °C. The transition temperature of YSZ decreases from 550 to 400 °C when doping with 10–20 vol.% LSM. The activation energy of conduction in 10 vol.% LSM–YSZ composite below and above 400 °C is 6.6 and 106 kJ mol^{-1}, respectively. The activation energy of conduction in 20 vol.% LSM–YSZ composite is nearly the same as that of 10 vol.% LSM–YSZ composite.

As the percolation limit (~20 vol.% LSM) is reached, the conduction is completely dominated by LSM phase. That means the hole and oxygen vacancy may play important roles in conduction. The electrical conductivity of LSM–YSZ increases from 4×10^{-2} to 2.27 S cm^{-1} at 1000 °C as the content of LSM increases from 10 to 50 vol.%. The activation energy of 30 and 40 vol.% LSM–YSZ composites is 16.1 and 16.3 kJ mol^{-1} while that of 50 vol.% LSM–YSZ is 9.0 kJ mol^{-1}, which is very close to that of pure LSM (Fig. 8).

As mentioned previously, the hole and oxygen vacancy both make contribution to the electrical conductivity of LSM–YSZ composites. The density of triple phase boundary is increased through the combination of composite structure. The reduction of oxygen molecule not only takes place at TPB but also on the entire surface of cathode composite. It is suggested that a functional cathode layer consisting of LSM–YSZ in a ratio of 30–70 vol.% should

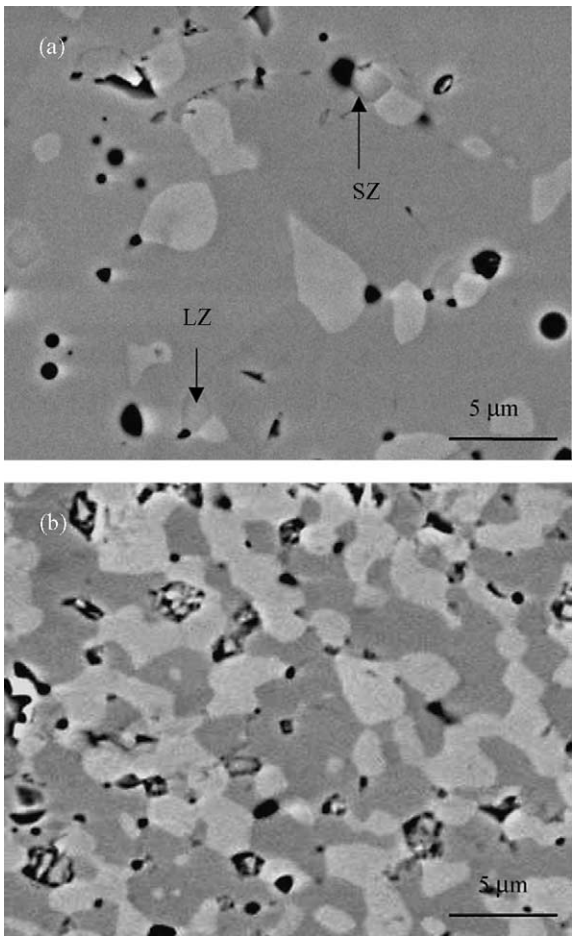

Fig. 10. SEM images of (a) 20 vol.% and (b) 50 vol.% LSM–YSZ composites, which were sintered at 1400 °C for 24 h.

provide optimized electrical conductivity and electrochemical behavior in the present research.

Fig. 10 shows the SEM images of 20 and 50 vol.% LSM–YSZ cathode composites, which were sintered at 1400 °C for 24 h. The SEM images show that porous LSM–YSZ composite is obtained. In 20 vol.% LSM–YSZ composite system, the brighter phase is LSM, which is dispersed in the YSZ matrix while the darker continuous phase is YSZ. Both phases form continuous features while increasing the content of LSM phase, as shown in Fig. 10b. Moreover, the formation of secondary phase such as $La_2Zr_2O_7$ (LZ) and $SrZrO_3$ (SZ) is occasionally found in 20 vol.% LSM–YSZ system, as indicated in Fig. 10a. Based on our previous publication [12], we proposed that the formation of LZ and SZ was due to the diffusion of Mn to YSZ. As the content of Mn in LSM is lower than the threshold value, the LSM becomes unstable, resulting in the occurrence of excessive La and Sr, and leading to the reaction of Zr with La and Sr. As the LSM content increases from 20 to 50 vol.%, more Mn ions is available and the LSM phase is stable. That makes the reaction between LSM and YSZ less pronounced although the diffusion of Mn to YSZ still takes place. Therefore, LZ or SZ is seldom found in 50 vol.% LSM–YSZ system.

4. Conclusions

1. Dense YSZ, containing 7.52 ± 0.15 mol% Y_2O_3 consists of equiaxial grains. The grain size of YSZ is about 5.5 μm. A little glassy phase, consisted of SiO_2 with minor Al_2O_3 is found in YSZ.
2. Two conducting species responsible for the ionic conduction of YSZ are $Y'_{Zr}V_O^{\bullet\bullet}$ and $V_O^{\bullet\bullet}$ dominating below and above the transition temperature of 550 °C. The electrical conductivity of YSZ is 6.67×10^{-2} S cm^{-1} at 1000 °C. The activation energy of the ionic conduction is 103 and 93 kJ mol^{-1} below and above the transition temperature, respectively. Three semi-circles are found and correspond to electrode, grain boundary and grain interior in the Cole–Cole plots.
3. The electrical conductivity of $La_{0.65}Sr_{0.3}MnO_3$ is 0.2 S cm^{-1} at room temperature. The conductivity of LSM increases with increasing the temperature. The activation energy for conduction is 9.6 kJ mol^{-1} in the ranges of testing temperature, which imply one conductive mechanism is dominant. Moreover, the impedance results show the conductivity of LSM is independent of the testing frequency from 200 to 1000 °C.
4. The conductivity of LSM–YSZ cathode composites is dominated either by YSZ or LSM for the lean and rich contents of LSM phases. For 10 and 20 vol.% LSM–YSZ composites, the hole and oxygen vacancy dominate the conduction below and above the transition temperature of 400 °C. As the percolation limit is reached (∼20 vol.% LSM), the conduction is completely controlled by the LSM phase.

Acknowledgements

The authors would like to thank the financial support under the contract NSC 90-2216-E-002-028 and DAAD PPP Project 91-2911-1-002-007. Also, the authors gratefully acknowledge Mr. Eduard Volz for his help in the measurement of the electrical conductivity.

References

[1] E.P. Murray, T. Tsai, S.A. Barnett, Oxygen transfer process in (La, Sr)MnO_3/Y_2O_3-stabilized ZrO_2 cathodes: an impedance spectroscopy study, Solid State Ionics 110 (1998) 235–243.
[2] T. Tsai, S.A. Barnett, Effect of LSM–YSZ cathode on thin-electrolyte solid oxide fuel cell performance, Solid State Ionics 93 (1997) 207–217.
[3] J.H. Kim, G.M. Choi, Mixed ionic and electronic conductivity of $[(ZrO_2)_{0.92}(Y_2O_3)_{0.08}]_{1-y}\cdot(MnO_{1.5})_y$, Solid State Ionics 130 (2000) 157–168.

[4] K. Hayashi, O. Yamamoto, Y. Nishigaki, H. Minoura, Sputtered $La_{0.5}Sr_{0.5}MnO_3$-yttria-stabilized-zirconia composite film electrodes for SOFC, Solid State Ionics 98 (1997) 49–55.
[5] Y.M. Park, G.M. Choi, Microstructure and electrical properties of YSZ–NiO composites, Solid State Ionics 120 (1999) 265–374.
[6] Y.C. Hsiao, J.R. Selman, The degradation of SOFC electrodes, Solid State Ionics 98 (1997) 33–38.
[7] H. Taimatsu, K. Wada, H. Kaneko, Mechanism of reaction between lanthanum manganite and yttria-stabilized zirconia, J. Am. Ceram. Soc. 75 (2) (1992) 401–405.
[8] N.Q. Minh, Ceramic fuel cells, J. Am. Ceram. Soc. 76 (3) (1993) 563–588.
[9] K. Wiik, C.R. Schmidt, S. Faaland, S. Shamsili, M.-A. Einarsrud, T. Grande, Reactions between strontium-substituted lanthanum maganite and yttria-stabilized zirconia. Part I. Powder samples, J. Am. Ceram. Soc. 82 (3) (1999) 721–728.
[10] K. Kleveland, M.-A. Einarsrud, C.S. Schmidt, S. Shamsili, S. Faaland, K. Wiik, T. Grande, Reactions between strontium-substituted lanthanum manganite and yttria-stabilized zirconia. Part II. Diffusion couples, J. Am. Ceram. Soc. 82 (3) (1999) 729–734.
[11] S. Faaland, M.-A. Einarsrud, K. Wiik, T. Grande, Reactions between $La_{1-x}Ca_xMnO_3$ and CaO-stabilized ZrO_2. Part I. Powder mixtures, J. Mater. Sci. 34 (1999) 957–966.
[12] C.-C.T. Yang, W.J. Wei, A. Roosen, Reaction kinetics and mechanism between $La_{0.65}Sr_{0.3}MnO_3$ and 8 mol% yttria-stabilized zirconia, J. Am. Ceram. Soc., 2002 (revised).
[13] S. Faaland, M.-A. Einarsrud, K. Wiik, T. Grande, Reactions between $La_{1-x}Ca_xMnO_3$ and CaO-stabilized ZrO_2. Part II. Diffusion couples, J. Mater. Sci. 34 (1999) 957–966.
[14] H.Y. Lee, S.M. Oh, Origin of cathodic degradation and new phase formation at the $La_{0.9}Sr_{0.1}MnO_3$/YSZ interface, Solid State Ionics 90 (1996) 133–140.
[15] C.-C.T. Yang, H.J. Cho, W.J. Wei, Quantitative characterization of various tetragonal zirconia polycrystals (TZPs), J. Eur. Ceram. Soc. 22 (2002) 199–207.
[16] M. Hirano, M. Inagaki, Improvement of mechanical and electrical properties of scandia-doped zirconia ceramics by post-sintering with hot isostatic pressing, J. Am. Ceram. Soc. 83 (10) (2000) 2619–2621.
[17] C. Petot, M. Filal, A.D. Rizea, K.H. Westmacott, J.Y. Lavol, C. Lacour, R. Ollitrault, Microstructure and ionic conductivity of freeze-dried yttria-doped zirconia, J. Eur. Ceram. Soc. 18 (1998) 1419–1428.
[18] S.P.S. Badwal, J. Drenann, Yttria-zirconia: effect of microstructure on conductivity, J. Mater. Sci. 22 (1987) 3231–3239.
[19] S.P.S. Badwal, Electrical conductivity of single crystal and polycrystalline yttria-stablized zirconia, J. Mater. Sci. 19 (1984) 1767–1776.
[20] S.P.S. Badwal, Grain boundary resistivity in zirconia-based materials: effect of sintering temperatures and impurities, J. Mater. Sci. 76 (1995) 67–80.
[21] M. Filal, C. Petot, M. Mokchah, C. Chateau, J.L. Charpentier, Ionic conductivity of yttrium-doped zirconia and the composite effect, Solid State Ionics 80 (1995) 27–35.
[22] N. Bonanos, B.C.H. Steele, E.P. Butler, W.B. Johnson, W.L. Worrell, D.D. Macdonald, M.C.H. Mckubre, Applications of impedance spectroscopy, in: J.R. Macdonald (Ed.), Impedance Spectroscopy: Emphasizing Solid Materials and Systems, Wiley, New York, 1987, pp. 215–230.
[23] S. Fritsch, A. Navrotsky, Thermodynamic properties of manganese oxides, J. Am. Ceram. Soc. 79 (7) (1996) 1761–1768.
[24] Y. Wu, T. Yu, B.S. Dou, C.X. Wang, X.F. Xie, Z.L. Yu, S.R. Fan, Z.R. Fan, L.C. Wang, A comparative study on perovskite-type mixed oxide catalysts $A'_xA_{1-x}BO_{3-\lambda}$ ($A' = Ca, Sr, A = La, B = Mn, Fe, Co$) for NH_3 oxidation, J. Catal. 120 (1989) 88–107.